PHYSICAL REVIEW B **76**, 075413 (2007)

Ab initio study of charge transport through single oxygen molecules in atomic aluminum contacts

S. Wohlthat,[1,2,*] F. Pauly,[1,2] J. K. Viljas,[1,2] J. C. Cuevas,[1,2,3] and Gerd Schön[1,2]

[1]*Institut für Theoretische Festkörperphysik and DFG Center for Functional Nanostructures, Universität Karlsruhe, D-76128 Karlsruhe, Germany*

[2]*Institut für Nanotechnologie, Forschungszentrum Karlsruhe, D-76021 Karlsruhe, Germany*

[3]*Departamento de Física Teórica de la Materia Condensada C-V, Universidad Autónoma de Madrid, E-28049 Madrid, Spain*

(Received 17 February 2007; revised manuscript received 15 May 2007; published 13 August 2007)

We present *ab initio* calculations of transport properties of atomic-sized aluminum contacts in the presence of oxygen. The experimental situation is modeled by considering a single oxygen atom (O) or one of the O_2 and O_3 molecules bridging the gap between electrodes forming ideal, atomically sharp pyramids. The transport characteristics are computed for these geometries with increasing distances between the leads, simulating the opening of a break junction. To facilitate comparison with experiments further, the vibrational modes of the oxygen connected to the electrodes are studied. It is found that in the contact regime, the change of transport properties due to the presence of oxygen is strong and should be detectable in experiments. All three types of oxygen exhibit a comparable behavior in their vibrational frequencies and conductances, which are well below the conductance of pure aluminum atomic contacts. The conductance decreases for an increasing number of oxygen atoms. In the tunneling regime, the conductance decays exponentially with distance and the decay length depends on whether or not oxygen is present in the junction. This fact may provide a way to identify the presence of a gas molecule in metallic atomic contacts.

DOI: 10.1103/PhysRevB.76.075413 PACS number(s): 73.23.−b, 72.10.−d, 71.15.−m, 63.22.+m

I. INTRODUCTION

Since the first experiments on atomic contacts, the "atmospheric" surroundings are known to have a strong effect on their charge transport properties.[1] Thus, studying the influence of adsorbed gas molecules is of great importance for the design of functional molecular-scale electronic components. It also shows some promise for the future development of gas sensors for "electronic noses." However, the systematic experimental investigation of the influence of single gas molecules on charge transport through metallic atomic contacts started only a few years ago with hydrogen in atomic platinum contacts.[2,3] It was found that the zero-bias conductance through such platinum-hydrogen contacts tends to be close to the quantum of conductance $G_0=2e^2/h$. In addition, this conductance value is due to a single, almost fully transparent channel.[2,4] Theoretical work has mostly confirmed these findings.[3,5–8]

Even so, one of the main problems in experiments of this type is to know if and in which configuration gas molecules are present in the contact region. A definite identification of the presence and the type of gas can be based on statistical techniques, such as the measurement of conductance histograms.[2,9] For individual contacts, this becomes much harder. In the experiments of Refs. 2 and 3, the identification of a single hydrogen molecule was based on the so-called inelastic point contact spectroscopy, where the local vibrational modes can be seen in the current-voltage (*I-V*) characteristics as abrupt features at bias voltages corresponding to the energies of the vibrations.[9] The evolution of these features with stretching of the contacts can then be compared to calculations of the vibrational modes for given configurations of the molecule.[2,3] In fact, theoretical methods have recently been developed that enable a direct comparison between the full experimental and theoretical *I-V* characteristics, including the inelastic signatures of the vibrational modes.[10–15]

For this purpose, namely, to identify small molecules in atomic metal contacts through transport measurements, we study the general properties of oxygen (O) in atomic aluminum (Al) contacts. In this paper, we concentrate on the behavior of the zero-bias transport characteristics when the atomic contacts are stretched. In the spirit of Refs. 2, 3, and 6, we also study the evolution and character of the vibrational modes. Aluminum was chosen because it becomes superconducting below temperatures of 1 K. As a result, in addition to measurements of the total zero-bias conductance, it is possible to determine experimentally the transmission eigenvalues of the individual channels from the *I-V* characteristics in the superconducting state.[16] As particular examples, we study single oxygen atoms (O), oxygen dimers (O_2), and ozone (O_3). These molecules (we also refer to the oxygen atom as a molecule) are placed initially in the middle of the contact between two aluminum electrodes, since their effect on the transport properties is then at its largest. We describe our contacts at the level of density-functional theory (DFT). In particular, the DFT electronic structure is employed to determine the charge transport properties by means of Green's function techniques.

In the following, we present stable structures of the three types of contacts, where oxygen molecules bridge the gap between two idealized aluminum electrodes. For them, we calculate the vibrational modes and the low-temperature transport properties, including the characterization of the individual transmission channels. We find that the energies of the vibrational modes, as well as the evolution of the conductance with increasing electrode distance, show qualitatively comparable characteristics for the three investigated molecules. In contrast to pure Al, the conductances of the Al-O_x-Al contacts are always well below $1G_0$, and for an

increasing number of O atoms, the conductance decreases. Moreover, the exponential decay lengths in the tunneling regime are different in the presence and in the absence of oxygen.

This paper is organized as follows. In Sec. II, we begin by presenting the methods used for determining the electronic structure, the geometries, and the transport properties of the molecular contacts. In Sec. III, we then describe the optimized geometries and the corresponding vibrational modes. Following this, Sec. IV relates in detail the transmission properties of the junctions to the relevant molecular orbitals. The section ends with an analysis of the evolution of the conductances when the contacts are opened. In particular, we analyze the tunneling regime, which is discussed further in the Appendix. In Sec. V, we conclude with the discussion of our results.

II. METHOD

In this section, we briefly present our methods for computing the electronic structures, geometries, and vibrational modes, as well as the charge transport characteristics of atomic contacts. A more detailed account will be given elsewhere.[17]

We describe our contacts at the level of DFT as implemented in the quantum chemistry package TURBOMOLE V5.7.[18–21] In particular, we use the "ridft" module[22,23] with the BP86 exchange-correlation functional[24,25] and a Gaussian basis set of split valence plus polarization (SVP) quality.[26] To be precise, polarization functions are present on all nonhydrogen atoms within the employed basis set. The total energy is converged to a precision of 10^{-6} hartree. Geometry optimization is performed until the maximum norm of the Cartesian gradient has fallen below 10^{-4} a.u. Vibrational modes in our contacts are determined using the "aoforce" module of TURBOMOLE.[27–29]

The investigated atomic contacts consist of two atomically sharp electrode tips and a single oxygen molecule connecting them (Fig. 1). The electrodes are Al fcc pyramids oriented in the (111) direction with a lattice constant of 4.05 Å and consist of at least four layers. While the outer layers are kept fixed all the time, the inner two layers of the freestanding pyramids are relaxed to find an energy minimum. Afterward, the atoms in the Al pyramids are kept fixed. Between two such electrodes, we place one representative oxygen molecule (O, O_2, or O_3). The molecule is then relaxed between the fixed electrodes, leading to a stable configuration. Starting from this first configuration, we move the electrodes stepwise further away from each other and relax the oxygen molecule again in each step. For each relaxed structure, we determine the vibrational modes of the molecule connected to the leads.

To compute the charge transport through a molecule between metallic electrodes, we apply a method based on standard Green's function techniques and the Landauer formula expressed in terms of a local nonorthogonal basis.[11,30–34] Due to the locality of the basis, the system is conveniently separated into three parts, leading to a single-particle Hamiltonian (or Fock matrix) of the molecular junction that has the following form:

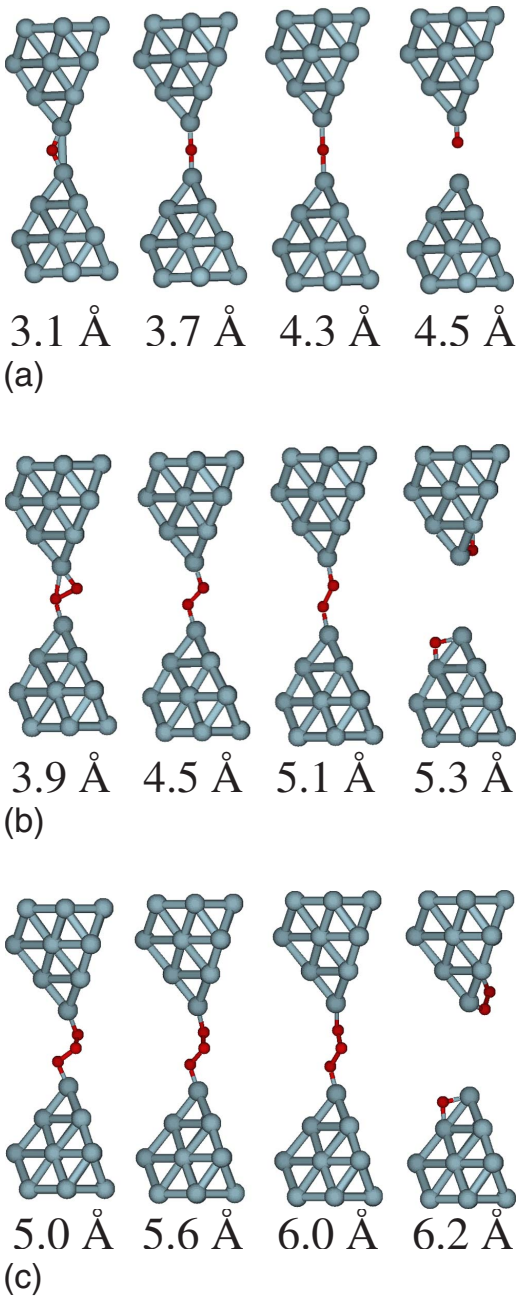

FIG. 1. (Color online) Al_{17}-O_x-Al_{17}: Optimized contact geometries and their tip-to-tip distances as obtained by stretching an aluminum (blue) atomic contact in the presence of oxygen (red) molecules. The Al pyramids consist of seven, six, three, and one atoms in the layers from the outside to the inside. (a) Al-O-Al, (b) Al-O_2-Al, (c) Al-O_3-Al.

$$\boldsymbol{H} = \begin{pmatrix} \boldsymbol{H}_{LL} & \boldsymbol{H}_{LC} & \boldsymbol{H}_{LR} \\ \boldsymbol{H}_{CL} & \boldsymbol{H}_{CC} & \boldsymbol{H}_{CR} \\ \boldsymbol{H}_{RL} & \boldsymbol{H}_{RC} & \boldsymbol{H}_{RR} \end{pmatrix}. \tag{1}$$

Here, $\boldsymbol{H}_{CC}$ describes the central system (C) consisting of the molecule and the tips of the electrodes and $\boldsymbol{H}_{XX}$, with $X=L,R$, describe the left (L) and right (R) electrodes. The matrices $\boldsymbol{H}_{LC}=\boldsymbol{H}_{CL}^{T}$, etc., give the hopping elements between

the different subsystems, but the hoppings between L and R are assumed to vanish ($\boldsymbol{H}_{LR}=\boldsymbol{H}_{RL}=\boldsymbol{0}$). This assumption has been verified in all our calculations, where the Hamiltonian elements connecting L and R were always smaller than 10^{-6} hartree. The overlap matrix $\boldsymbol{S}$ of the nonorthogonal basis has a similar structure.

The conductances of the molecular junctions are determined by means of Green's function techniques. The low-temperature zero-bias conductance $G=dI/dV|_{V=0}$ is given by the Landauer formula

$$G = G_0 \mathrm{Tr}[\boldsymbol{t}(E_F)\boldsymbol{t}^{\dagger}(E_F)] = G_0 T(E_F), \tag{2}$$

where $\boldsymbol{t}(E_F)$ is the transmission matrix of the molecular junction evaluated at the Fermi energy E_F. The total transmission at any energy E can be written as $T(E)=\Sigma_{n=1}^{\infty} T_n(E)$, where $T_n(E)$ are the transmissions of the individual eigenchannels, defined as the eigenvalues of $\boldsymbol{t}(E)\boldsymbol{t}^{\dagger}(E)$. The transmission matrix can be calculated in terms of Green's functions of the molecular junction as follows:[35]

$$\boldsymbol{t}(E) = 2\boldsymbol{\Gamma}_L^{1/2}(E)\boldsymbol{G}_{CC}^{r}(E)\boldsymbol{\Gamma}_R^{1/2}(E). \tag{3}$$

Here,

$$\boldsymbol{G}_{CC}^{r}(E) = [E\boldsymbol{S}_{CC} - \boldsymbol{H}_{CC} - \boldsymbol{\Sigma}_L^{r}(E) - \boldsymbol{\Sigma}_R^{r}(E)]^{-1} \tag{4}$$

is the retarded Green's function of the central system, and $\boldsymbol{\Gamma}_X(E)=-\mathrm{Im}[\boldsymbol{\Sigma}_X^{r}(E)]$ are the scattering rate matrices. These depend on the self-energy matrices

$$\boldsymbol{\Sigma}_X^{r}(E) = (\boldsymbol{H}_{CX} - E\boldsymbol{S}_{CX})\boldsymbol{g}_{XX}^{r}(E)(\boldsymbol{H}_{XC} - E\boldsymbol{S}_{XC}), \tag{5}$$

where $\boldsymbol{g}_{XX}^{r}(E)$ is the retarded surface Green's functions of the electrode $X=L,R$, which are modeled as ideal surfaces. These self-energies contain all the information about the electronic structure of the electrodes and their coupling to the central system.

The electronic structure of the central system and its coupling to the electrodes are obtained from the calculated geometries (Fig. 1). Let us refer to these geometries, which consist of the two pyramids bridged by a molecule, as "contact geometries." These contact geometries are divided into three parts. The central part, corresponding to region C in the transport calculation, consists of the molecule and the inner two layers of the pyramids. The excluded outer layers on the left and right sides are used for calculating the hoppings and overlaps between the central region and the electrodes, as needed in Eq. (5).

To obtain the surface Green's functions $\boldsymbol{g}_{XX}^{r}(E)$, we compute separately the electronic structure of a spherical Al fcc cluster with 555 atoms. From this, we extract the Fock and overlap matrix elements between the atom in the origin of the cluster and all its neighbors and, using these "bulk parameters," construct a semi-infinite periodic crystal. The surface Green's functions are then calculated from this crystal using the so-called decimation technique.[36] We have checked that the electrode construction in the employed nonorthogonal SVP basis set has converged with respect to the size of the Al cluster, from which we extract our parameters.[17] In this way, we describe the whole system consistently within DFT, using the same basis set and exchange-correlation functional everywhere.

The Fermi energy E_F of the coupled system, namely, the C part connected to the semi-infinite electrodes, required to determine the conductance [Eq. (2)], is assumed to be given by the Al leads. We obtain its value as the average of the energies of the highest occupied (−4.261 eV) and the lowest unoccupied (−4.245 eV) orbitals of the bulk cluster. In this way, we find $E_F=-4.25$ eV. The same quantity for the contact geometries deviates from this bulk value by less than 0.08 eV. Let us stress that the Fermi energy is only used to read off the conductance from a transmission function $T(E)$ but does not enter into our calculations otherwise.

III. CONTACT GEOMETRIES AND VIBRATIONAL MODES

We simulate the opening of a contact for the three most basic forms of oxygen (O, O_2, and O_3). Figure 1 shows a selection of the relaxed geometries obtained, the starting configuration, one halfway, the one just before, and the one directly after the breaking. In the case of a single O atom, the O sits at first on the side of the Al dimer contact. Upon stretching, this atom moves onto the contact axis and stays symmetrically bonded to both pyramids until the contact breaks [Fig. 1(a)]. When the contact is broken, the oxygen atom binds to one electrode with a distance of approximately 1.7 Å on top of the pyramid and stays bonded like this. However, this binding position is only metastable. If one distorts the position of the oxygen atom slightly, e.g., places it at some distance from the contact axis, and optimizes the contact geometry again, the atom goes to one side of the pyramid in the same way as for O_2 and O_3 described below. This position with the oxygen bonded to one side of the pyramid is energetically favored by approximately 2.5 eV. In the case of O_2, the molecular axis of the oxygen molecule is almost perpendicular to the contact axis in the beginning and rotates afterward into this axis [Fig. 1(b)]. For O_3, the molecule is twisted around the contact axis. This twist contracts toward the contact axis when the contact is stretched [Fig. 1(c)]. In the cases of Al-O_2-Al and Al-O_3-Al, the O atoms move always to the sides of the pyramids when the contact is broken. The evolution of the distances between the atoms while opening the contact is shown in Table I.

As mentioned above, in order to compare with results from inelastic transport experiments, we also calculate the vibrational modes of the oxygen molecules in the contact. Since the atomic mass of Al is almost twice as large as that of O, it is a reasonable first approximation to neglect the motion of the Al atoms, which is what our model assumes. The energies of the vibrational modes for the different structures are shown in Fig. 2. For these structures, the modes can be classified roughly as being longitudinal or transverse, according to the motions of the atoms relative to the axis of the contact. The mode energies are in the range of 50–140 meV for Al-O-Al. The two transverse modes are more or less constant around 50 meV, while the longitudinal mode increases from 120 to a maximum of 140 meV at a distance of 3.3 Å and drops afterward almost linearly. For Al-O_2-Al, the mode

TABLE I. Distances between the aluminum tip atoms and the lengths of the individual Al-O, O-O, and O-Al bonds for the contact geometries depicted in Fig. 1.

(a) Al-O-Al

Al-Al	Al-O	O-Al
3.097 Å	1.700 Å	1.700 Å
3.297 Å	1.685 Å	1.685 Å
3.497 Å	1.749 Å	1.749 Å
3.697 Å	1.849 Å	1.849 Å
3.897 Å	1.948 Å	1.948 Å
4.097 Å	2.048 Å	2.048 Å
4.297 Å	2.150 Å	2.147 Å
4.497 Å	2.779 Å	1.718 Å

(b) Al-O_2-Al

Al-Al	Al-O	O-O	O-Al
3.938 Å	1.812 Å	1.571 Å	1.796 Å
4.138 Å	1.785 Å	1.535 Å	1.785 Å
4.338 Å	1.783 Å	1.503 Å	1.787 Å
4.538 Å	1.799 Å	1.486 Å	1.803 Å
4.738 Å	1.828 Å	1.488 Å	1.830 Å
4.938 Å	1.867 Å	1.511 Å	1.869 Å
5.138 Å	1.900 Å	1.571 Å	1.899 Å

(c) Al-O_3-Al

Al-Al	Al-O	O-O	O-O	O-Al
4.970 Å	1.798 Å	1.471 Å	1.461 Å	1.802 Å
5.170 Å	1.802 Å	1.464 Å	1.456 Å	1.806 Å
5.370 Å	1.809 Å	1.461 Å	1.454 Å	1.813 Å
5.570 Å	1.820 Å	1.463 Å	1.456 Å	1.822 Å
5.770 Å	1.833 Å	1.469 Å	1.464 Å	1.835 Å
5.970 Å	1.855 Å	1.486 Å	1.476 Å	1.858 Å

energies are in the range of 40–150 meV. The two lowest modes are transverse and constant in energy. The highest mode is longitudinal and increases from 135 to 150 meV at 4.5 Å and drops afterward to 120 meV. The other three modes lie in the range of 70–110 meV. For Al-O_3-Al, the lowest (transverse) modes lie constant at an energy of approximately 25 meV. The highest (longitudinal) mode increases first to its maximum of 160 meV at 5.4 Å and decreases afterward. Another mode lies close to this highest one. All other modes have energies between 50 and 120 meV.

The behavior of the vibrational energies can be understood by re-examining the atomic distances in the geometries (Table I). Despite the fact that the atomic contacts are being stretched, it happens, for example, that in the beginning, some atoms move closer together. Therefore, certain bonds strengthen due to this bond shortening, and corresponding modes may show an initial increase in their vibrational frequencies.

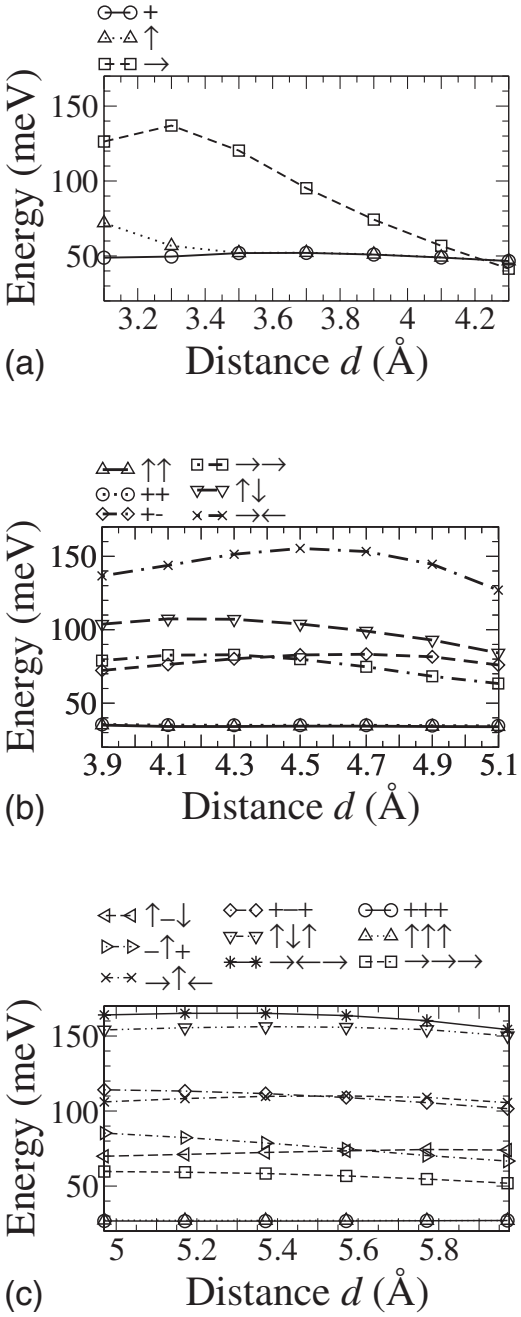

FIG. 2. Al-O_x-Al: Energy of the vibrational modes of the oxygen molecule connected to Al pyramids as a function of the distance d between the Al tip atoms. The arrows and plus and minus signs denote the directions of relative displacements of the atoms in a given mode: → and ← denote motion along the axis of the contact while +,− and ↑,↓ denote motion in the two directions perpendicular to the axis. (a) Al-O-Al, (b) Al-O_2-Al, (c) Al-O_3-Al.

IV. TRANSPORT PROPERTIES AND ELECTRONIC STRUCTURE

Before we determine the transport properties for the different forms of oxygen between aluminum electrodes, we will show the results for a pure Al atomic contact. The transmission as a function of energy and the corresponding contact geometry are plotted in Fig. 3. The conductance of this

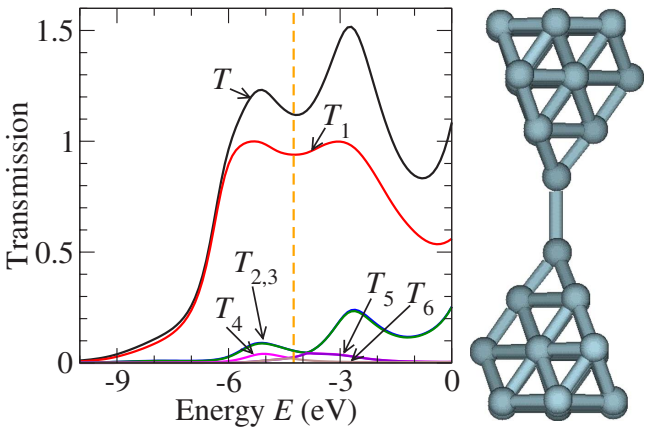

FIG. 3. (Color online) Al-Al: Transmission as a function of energy. Both the total transmission (T) and its channel contributions (T_n) are shown. The vertical dashed line indicates the Fermi energy of bulk Al. The corresponding contact geometry with a distance of 3.4 Å between the Al tip atoms is depicted on the right.

contact is close to $1G_0$ and is carried by three channels, as expected.[16,37–39] If oxygen sits between the two electrodes, the transmission changes significantly. The resulting $T(E)$ curves for the contact geometries of Fig. 1 are shown in Fig. 4. We note that whenever we speak about numbers of channels in this work, we mean channels that contribute at least 5% to the total conductance. This criterion approximately agrees with what can be resolved experimentally using superconducting electrodes.[16]

The total transmissions $T(E)=\Sigma_n T_n(E)$ and the transmission eigenvalues $T_n(E)$ of the individual channels of Al-O-Al [Fig. 1(a)] are plotted as a function of energy E in the left column of Fig. 4. The peaks labeled 1–3 below the Fermi energy are due to oxygen. This can be seen from the local density of states (LDOS) shown for a tip-to-tip distance of 3.7 Å in Fig. 5,[40] as well as from the orbitals at the peaks shown in Fig. 6. Peak 1 corresponds to the p_z orbital of O (z is the transport direction). Peaks 2 and 3 become almost degenerate as soon as the O is on the contact axis. These peaks are due to the p_x and p_y orbitals of O. Peak 1 is broader and shifted to lower energies than peaks 2 and 3 due to the stronger binding of the p_z orbital to the Al states. The peaks above the Fermi energy are due to aluminum. The number of channels contributing to the conductance is at least 3. When the contact is opened, peaks 1–3 move, up to a tip-to-tip distance of 3.3 Å, away from and afterward toward the Fermi energy. This behavior is caused by the length of the Al-O bond.

For Al-O_2-Al [Fig. 1(b)], the total transmission and the channel transmissions are shown in the central column of Fig. 4. The peaks in $T(E)$ are caused by the oxygen, as can be seen from the LDOS in Fig. 5 for a tip-to-tip distance of 4.5 Å. Peaks 4 and 5 originate from the antibonding π orbitals and peak 6 from the antibonding σ orbital (Fig. 6). The number of channels at the Fermi energy is 2 for the intermediate tip-to-tip distances between 4.6 and 4.9 Å, but otherwise 3. Peaks 4 and 5 shift upward in energy without crossing the Fermi energy while the contact is stretched. Peak 6 moves first away from and then, after a tip-to-tip distance of

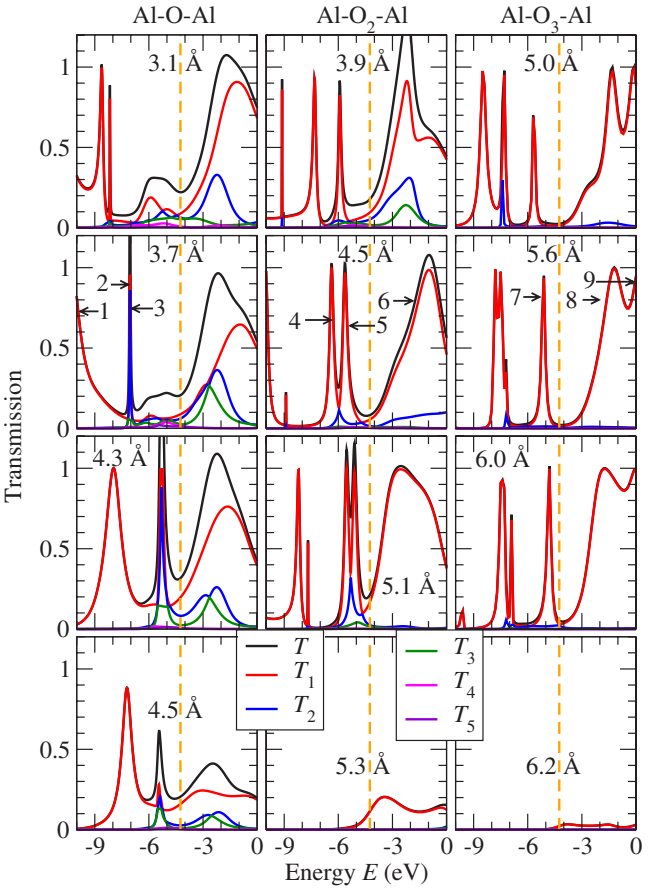

FIG. 4. (Color online) Al-O_x-Al: Transmission as a function of energy for the structures shown in Fig. 1. The tip-to-tip distance increases from the top to the bottom and is given in the panels. The vertical dashed lines indicate the Fermi energy.

4.5 Å, toward the Fermi energy. The movement of this peak can be understood in terms of the behavior of the distance between the O atoms, while the length of the Al-O bond is mainly responsible for the displacement of peaks 4 and 5.

For Al-O_3-Al [Fig. 1(c)], the transmissions are plotted in the right column of Fig. 4. The peaks shown have their origin in the ozone (Figs. 5 and 6). Peaks 8 and 9 move away from the Fermi energy with stretching up to a tip-to-tip distance of 5.4 Å and approach afterward the Fermi energy. Peak 7

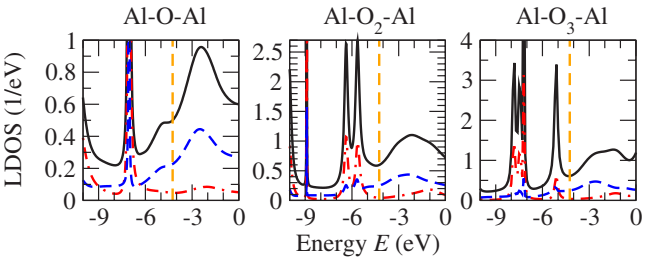

FIG. 5. (Color online) Al-O_x-Al: LDOS corresponding to the second row in Fig. 4. The solid (black) curve is for the region including the Al tip atoms and the O atoms, the dash-dotted (red) one is for one of the oxygen atoms, and the dashed (blue) curve is for one of the Al tip atoms. The vertical dashed (orange) line indicates the Fermi energy.

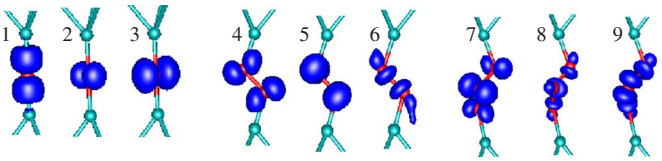

FIG. 6. (Color online) Al_{17}-O_x-Al_{17}: Orbitals of the contact geometries of Fig. 1. Orbitals 1–3 belong to Al_{17}-O-Al_{17} with a tip-to-tip distance of d=3.7 Å, orbitals 4–6 to Al_{17}-O_2-Al_{17} with d =4.5 Å, and orbitals 7–9 to Al_{17}-O_3-Al_{17} with d=5.6 Å. The energies of the orbitals are −10.537 eV (1), −7.238 eV (2), −7.176 eV (3), −6.274 eV (4), −5.606 eV (5), −2.133 eV (6), −5.197 eV (7), −2.175 eV (8), and +0.153 eV (9), where the number of the orbital is given in parentheses.

shifts continuously toward the Fermi energy. The movement of peaks 8 and 9 again reflects the distances between the oxygen atoms, and the shift of peak 7 changes in the Al-O bond length. The current is carried, up to a tip-to-tip distance of 5.4 Å, by three channels and afterward by two channels.

In Fig. 7, the conductance is plotted as a function of the tip-to-tip distance for pure Al and for the three different oxygen molecules in Al contacts. For pure Al contacts, we obtain a conductance close to $1G_0$ with a positive slope shortly before rupture of the contact, in agreement with previous investigations of Al atomic contacts.[16,39,41,42] In the presence of oxygen, the conductances show the same qualitative features for the three molecules (O, O_2, and O_3). The conductance first decreases with stretching up to a certain point. After this point, it increases rapidly until the contact breaks and the conductance drops. This trend can be understood by re-examining the evolution of the energy dependence of the transmission upon stretching (Fig. 4). Thus, for instance, the increase of the conductance originates from the fact that the highest occupied molecular orbitals move close to the Fermi energy. Quantitatively, the conductance depends on the number of oxygen atoms in the molecule. The more oxygen atoms, the lower the conductance. In all cases, the transport is influenced by a charge transfer from the Al to the oxygen molecule (around $-0.6e$ for all the three molecules, as determined by a Mulliken population analysis), leading to an occupation of molecular orbitals which would be empty in an isolated oxygen molecule. Therefore, current is carried by formerly unoccupied p orbitals.

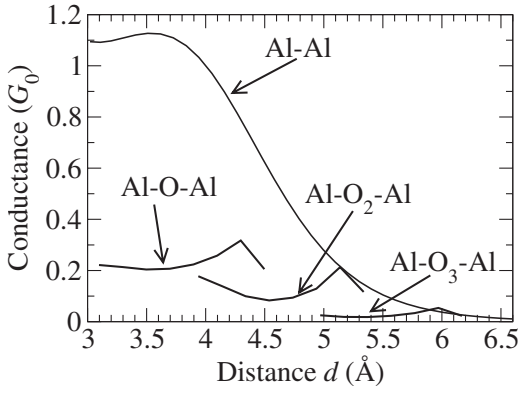

FIG. 7. Al-O_x-Al: Conductance as a function of the distance between the Al tip atoms.

We also investigate the conductance in the tunneling regime. With this term, we refer to the region of large tip-to-tip distances d, where the conductance exhibits an exponential decay $G(d)/G_0 \propto e^{-\beta d}$ with an inverse decay length β. In experiments, there might be any number of O molecules covering the surfaces of the Al pyramids, but we calculate representatively the tunneling conductance of Al-O_2-Al (not shown in Fig. 7), where the O atoms sit separated on both pyramids [see the rightmost part of Fig. 1(b)]. We compare this to the tunneling conductance of pure Al contacts (shown in Fig. 7). For pure Al, the inverse decay length turns out to be β=2.1 $Å^{-1}$ and for Al with an O atom on both pyramids, β=2.3 $Å^{-1}$. Thus, the decay of the conductance is somewhat faster when oxygen is present.

Physically, the value of β is determined by the shape of the potential barrier between the tips, especially its apparent height with respect to E_F.[43] The barrier depends sensitively on the electronic structure of the junction, including the charge-transfer effects between the different atoms close to the tips. In terms of the local basis picture, all this information is contained in the spectral functions of the tips and the hopping matrix elements connecting them. The mathematical details of this interpretation are discussed further in the Appendix. In this picture, an important role is played by the radial decay properties of the orbitals of the tip atoms that are relevant for transport. Roughly speaking, for O, these orbitals are the $2p$ ones, while for Al, they are of the $3s$ and $3p$ types. The former orbitals decay faster and, thus, it is reasonable that inverse decay length β is larger in the presence of oxygen. Although the oxygen-induced change in β in this particular example is not very large, we suggest that, in general, changes in the decay rate of the tunneling conductance may provide another possibility to check experimentally whether gas molecules are present in the atomic contact or not.

V. DISCUSSION AND CONCLUSIONS

Let us point out that we have checked that the results presented in this work are robust with respect to the size of the contacts. In particular, the charge transport characteristics do not change significantly when the size of the pyramids in the contact geometries is increased, nor do they depend sensitively on the partitioning into the L, C, and R regions. We illustrate this fact in Fig. 8, where we compare the transmission functions $T(E)$ of the Al-O_2-Al contact of Fig. 1(b) at a tip-to-tip distance of 4.5 Å. We vary the numbers of layers in the Al pyramids and divide the system differently into the three regions. Clearly, the essential features of the results remain unaffected by these modifications. Such a robustness is observed as long as the assumption about vanishing matrix elements between the L and R regions is fulfilled, and there are enough layers (at least two in the case of Al) left in the L and R parts of the pyramids for coupling the C part to the surfaces.

In order to investigate structures where the effect of O molecules on the transport properties is at its largest, we have placed the oxygen molecules initially between the pyramids and kept the Al electrodes fixed in the geometry-

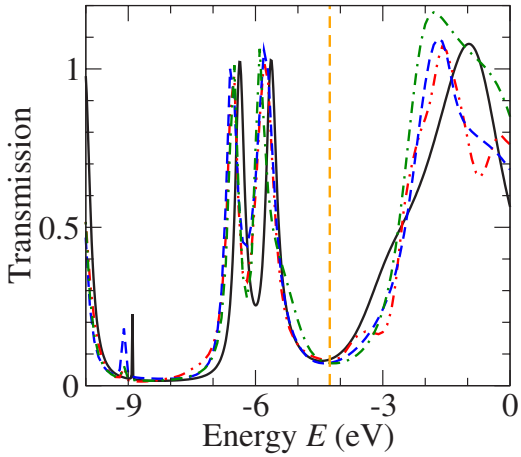

FIG. 8. (Color online) Robustness of the transmission for an Al-O_2-Al contact at a tip-to-tip distance of 4.5 Å [Fig. 1(b)]. Shown are $T(E)$ curves for an increased number of Al atoms in the pyramids, as well as for different partitionings of the contact into L, C, and R regions. The solid black line is the transmission of 7-6-|3-1-O_2-1-3|-6-7 (Fig. 4). The numbers stand for the Al atoms in each layer of the pyramid and "|" indicates how the system is divided into the three different regions. The dash-dot-dotted line corresponds to the system 6-12-|10-6-3-1-O_2-1-3-6-10|-12-6, the dashed line to 6-12-10-|6-3-1-O_2-1-3-6|-10-12-6, and the dash-dotted line to 6-12-10-6-|3-1-O_2-1-3|-6-10-12-6. The vertical dashed line indicates the Fermi energy.

optimization process. On the other hand, we know that relaxing parts of the pyramids together with the molecule can lead to geometrical structures differing considerably from the ideal contacts shown in Fig. 1. An example of such a geometry is depicted in Fig. 9. Moreover, the formed structures depend on the initial placements of the atoms close to the tips and on the number of oxygen molecules present. Different realizations of atomic configurations can also be observed in experiments, where various kinds of I-V characteristics have been measured.[44] However, as the transmission function in Fig. 9 shows, even more complex geometries can exhibit results whose main features resemble those of the simplified structures discussed above. The transmission function shown in this figure should be compared with the ones for the Al-O-Al contact in Fig. 4. In particular, similar to those results, there are three peaks (1–3) below the Fermi energy and the conductance is around $0.2G_0$.

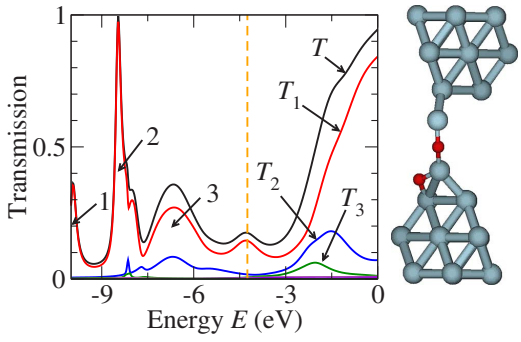

FIG. 9. (Color online) Al-O_2-Al: Example of a possible geometrical configuration when the Al tip atoms are included in the relaxation process in addition to the molecule, and the corresponding transmission as a function of energy. The vertical dashed line indicates the Fermi energy.

A similar approach to investigate oxygen in Al junctions was chosen by Jelínek *et al.*[42] Those authors found structures where an oxygen atom is incorporated into the electrodes and their electrodes are connected by an aluminum dimer in the final stage before the contact breaks. The conductance in their structures, therefore, is dominated by the aluminum dimer and the influence of the oxygen atom on the conductance is weak. We nevertheless believe that structures with oxygen molecules bridging the gap between Al electrodes can be found in experiments. A situation corresponding to our simulations would most likely arise when the oxygen is introduced into open contacts that are subsequently closed and then reopened. The experimental results can then be compared to our predictions.

In conclusion, we studied the charge transport properties of aluminum atomic contacts in the presence of oxygen molecules (O, O_2, and O_3). We obtained stable geometrical structures for the molecules in the junctions and determined the molecules' vibrational modes in the presence of the aluminum electrodes. In principle, these modes should be measurable with the methods of point contact spectroscopy. Moreover, we analyzed the evolution of the conductance for the Al-O/O_2/O_3-Al contacts in stretching processes, mimicking a conductance curve measured in experiments while opening a break junction. These results show a typical behavior for all the different molecules studied. First, the conductance decreases until it starts to increase shortly before the contact breaks. The value of the conductance was found to decrease with the number of oxygen atoms. Our observations can be understood by the interplay between mechanical and electronic properties. Changes in the distances between the atoms result in modifications of the electronic structure. The shifts in energy positions of individual molecular orbitals and their corresponding peaks in the transmission function can in turn explain the behavior of the conductance in the stretching processes. Finally, we studied the decay lengths of the conductance in the tunneling regime and found the decay to be faster in the presence of oxygen than for pure aluminum contacts. This effect may provide a way for detecting gas molecules in metallic atomic contacts.

ACKNOWLEDGMENTS

We would like to thank Michael Häfner, Marcelo Goffman, and Antoine Isambert for sharing their ideas with us. We also thank the Theoretical Chemistry group of Reinhart Ahlrichs for helpful discussions and for providing us with TURBOMOLE. Financial support by the Helmholtz Gemeinschaft within the "Nachwuchsgruppen-Programm" (Contract No. VH-NG-029), the Landesstiftung Baden-Württemberg within the "Kompetenznetz Funktionelle Nanostrukturen," and the DFG within the CFN is gratefully acknowledged.

APPENDIX: CONDUCTANCE FORMULA IN THE TUNNELING LIMIT

In the actual conductance calculations presented in this paper, we always use the formula given in Eq. (2). For a

better understanding of the tunneling regime, it is nevertheless useful to cast Eq. (2) into another well-known form. Let us assume that the C part of the system can be divided into regions 1 and 2, where region 1 (2) is not coupled to the R (L) lead through direct hoppings or overlaps. Furthermore, regions 1 and 2 are connected to each other by $\boldsymbol{t}_{12}=\boldsymbol{H}_{12}-E\boldsymbol{S}_{12}$. Equation (2) can then be written in the form

$$G = G_0 \,\mathrm{Tr}[\boldsymbol{G}^r_{12}(\boldsymbol{\Gamma}_R)_{22}\boldsymbol{G}^a_{21}(\boldsymbol{\Gamma}_L)_{11}], \tag{A1}$$

where $\boldsymbol{G}^a_{21}=(\boldsymbol{G}^r_{12})^\dagger$, and all energy-dependent quantities are evaluated at E_F. Let us denote by $\boldsymbol{g}^r_{11}$ and $\boldsymbol{g}^r_{22}$ the Green's functions for regions 1 and 2 in the absence of $\boldsymbol{t}_{12}$. For example, $\boldsymbol{g}^r_{11}(E)=[E\boldsymbol{S}_{11}-\boldsymbol{H}_{11}-(\boldsymbol{\Sigma}^r_L)_{11}]^{-1}$. We also define the unperturbed spectral density matrix $\boldsymbol{A}_{11}=i(\boldsymbol{g}^r_{11}-\boldsymbol{g}^a_{11})$, where $\boldsymbol{g}^a_{11}=(\boldsymbol{g}^r_{11})^\dagger$, with a similar definition for $\boldsymbol{A}_{22}$. We note that $\boldsymbol{H}_{11}$ and $\boldsymbol{H}_{22}$ are simply cut out from the full, self-consistent $\boldsymbol{H}_{CC}$, and thus still contain indirect effects of $\boldsymbol{t}_{12}$.

The full propagator between 1 and 2 is given by the Dyson equation[45] $\boldsymbol{G}^r_{12}=\boldsymbol{g}^r_{11}\boldsymbol{t}_{12}\boldsymbol{G}^r_{22}=\boldsymbol{g}^r_{11}\boldsymbol{T}_{12}\boldsymbol{g}^r_{22}$. In the last stage, we defined the t matrix $\boldsymbol{T}_{12}$ due to the perturbation $\boldsymbol{t}_{12}$.[46] Inserting these into Eq. (A1) and using the identities $\boldsymbol{g}^r_{11}(\boldsymbol{\Gamma}_L)_{11}\boldsymbol{g}^a_{11}=\boldsymbol{A}_{11}$ and $\boldsymbol{g}^r_{22}(\boldsymbol{\Gamma}_R)_{22}\boldsymbol{g}^a_{22}=\boldsymbol{A}_{22}$, we find the following formula:[47]

$$G = G_0 \,\mathrm{Tr}[\boldsymbol{T}_{12}\boldsymbol{A}_{22}\boldsymbol{T}_{21}\boldsymbol{A}_{11}]. \tag{A2}$$

Far in the tunneling regime, the quantities $\boldsymbol{t}_{12}$ are small, such that the lowest-order approximation $\boldsymbol{T}_{12}=\boldsymbol{t}_{12}$ should be valid. Furthermore, to lowest order, the electronic structures of the tips (as represented by $\boldsymbol{H}_{11}$ and $\boldsymbol{H}_{22}$, and hence $\boldsymbol{A}_{11}$ and $\boldsymbol{A}_{22}$) also become independent of the tip-to-tip distance.

The decay rate of the conductance with increasing distance between the tips (β) is now seen to be determined by two factors. The first is due to the decay of the couplings $\boldsymbol{t}_{12}$. If one uses the Wolfsberg-Helmholz (or "extended Hückel") approximation, then $\boldsymbol{H}_{12}$, and hence $\boldsymbol{t}_{12}$, are related in a simple way to the overlap $\boldsymbol{S}_{12}$.[48] This emphasizes that the major effect to the decay of $\boldsymbol{t}_{12}$ is simply due to the associated local basis functions, which decay with varying rates. The second factor is due to the spectral functions $\boldsymbol{A}_{11}$ and $\boldsymbol{A}_{22}$. They weight the various components of $\boldsymbol{t}_{12}$ differently, and thus finally determine the decay rate β. The physical quantity controlling this rate is still the effective tunneling barrier, in particular, its height with respect to E_F, because the latter determines the barrier-penetration lengths of the electronic eigenstates of the tips. This information is contained in the matrices $\boldsymbol{A}_{11}$ and $\boldsymbol{A}_{22}$ in the form of the weights of the different local basis functions of the tip atoms.

*Present address: School of Chemistry, The University of Sydney, Sydney, New South Wales 2006, Australia.

[1] J. K. Gimzewski and R. Möller, Phys. Rev. B **36**, 1284 (1987).
[2] R. H. M. Smit, Y. Noat, C. Untiedt, N. D. Lang, M. C. van Hemert, and J. M. van Ruitenbeek, Nature (London) **419**, 906 (2002).
[3] D. Djukic, K. S. Thygesen, C. Untiedt, R. H. M. Smit, K. W. Jacobsen, and J. M. van Ruitenbeek, Phys. Rev. B **71**, 161402(R) (2005).
[4] D. Djukic and J. M. van Ruitenbeek, Nano Lett. **6**, 789 (2006).
[5] J. C. Cuevas, J. Heurich, F. Pauly, W. Wenzel, and G. Schön, Nanotechnology **14**, R29 (2003).
[6] Y. García, J. J. Palacios, E. SanFabián, J. A. Vergés, A. J. Pérez-Jiménez, and E. Louis, Phys. Rev. B **69**, 041402(R) (2004).
[7] K. S. Thygesen and K. W. Jacobsen, Phys. Rev. Lett. **94**, 036807 (2005).
[8] V. M. García-Suárez, A. R. Rocha, S. W. Bailey, C. J. Lambert, S. Sanvito, and J. Ferrer, Phys. Rev. B **72**, 045437 (2005).
[9] N. Agraït, A. Levy Yeyati, and J. M. van Ruitenbeek, Phys. Rep. **377**, 81 (2003).
[10] T. Frederiksen, M. Brandbyge, N. Lorente, and A.-P. Jauho, Phys. Rev. Lett. **93**, 256601 (2004).
[11] J. K. Viljas, J. C. Cuevas, F. Pauly, and M. Häfner, Phys. Rev. B **72**, 245415 (2005).
[12] L. de la Vega, A. Martín-Rodero, N. Agraït, and A. L. Yeyati, Phys. Rev. B **73**, 075428 (2006).
[13] H. Ness, J. Phys.: Condens. Matter **18**, 6307 (2006).
[14] G. C. Solomon, A. Gagliardi, A. Pecchia, T. Frauenheim, A. Di Carlo, J. R. Reimers, and N. S. Hush, J. Chem. Phys. **124**, 094704 (2006).
[15] T. Frederiksen, M. Paulsson, M. Brandbyge, and A.-P. Jauho, Phys. Rev. B **75**, 205413 (2007).
[16] E. Scheer, P. Joyez, D. Esteve, C. Urbina, and M. H. Devoret, Phys. Rev. Lett. **78**, 3535 (1997).
[17] F. Pauly, Ph.D. thesis, Universität Karlsruhe, 2007; F. Pauly, J. K. Viljas, U. Huniar, M. Häfner, J. C. Cuevas, and G. Schön (unpublished).
[18] R. Ahlrichs, M. Bär, M. Häser, H. Horn, and C. Kölmel, Chem. Phys. Lett. **162**, 165 (1989).
[19] O. Treutler and R. Ahlrichs, J. Chem. Phys. **102**, 346 (1995).
[20] P. Hohenberg and W. Kohn, Phys. Rev. **136**, B864 (1964).
[21] W. Kohn and L. J. Sham, Phys. Rev. **140**, A1133 (1965).
[22] K. Eichkorn, O. Treutler, H. Öhm, M. Häser, and R. Ahlrichs, Chem. Phys. Lett. **242**, 652 (1995).
[23] K. Eichkorn, F. Weigend, O. Treutler, and R. Ahlrichs, Theor. Chem. Acc. **97**, 119 (1997).
[24] A. D. Becke, Phys. Rev. A **38**, 3098 (1988).
[25] J. P. Perdew, Phys. Rev. B **33**, 8822 (1986).
[26] A. Schäfer, H. Horn, and R. Ahlrichs, J. Chem. Phys. **97**, 2571 (1992).
[27] P. Deglmann and F. Furche, J. Chem. Phys. **117**, 9535 (2002).
[28] P. Deglmann, F. Furche, and R. Ahlrichs, Chem. Phys. Lett. **363**, 511 (2002).
[29] H. Horn, H. Weiss, M. Häser, M. Ehrig, and R. Ahlrichs, J. Comput. Chem. **12**, 1058 (1991).
[30] J. Taylor, H. Guo, and J. Wang, Phys. Rev. B **63**, 245407 (2001).
[31] P. S. Damle, A. W. Ghosh, and S. Datta, Phys. Rev. B **64**, 201403(R) (2001).
[32] M. Brandbyge, J.-L. Mozos, P. Ordejón, J. Taylor, and K. Stokbro, Phys. Rev. B **65**, 165401 (2002).
[33] Y. Q. Xue, S. Datta, and M. A. Ratner, Chem. Phys. **281**, 151 (2002).

[34] Y. Q. Xue and M. A. Ratner, Phys. Rev. B **68**, 115406 (2003).
[35] J. Heurich, J. C. Cuevas, W. Wenzel, and G. Schön, Phys. Rev. Lett. **88**, 256803 (2002).
[36] F. Guinea, C. Tejedor, F. Flores, and E. Louis, Phys. Rev. B **28**, 4397 (1983).
[37] J. C. Cuevas, A. L. Yeyati, and A. Martín-Rodero, Phys. Rev. Lett. **80**, 1066 (1998).
[38] R. Cron, M. F. Goffman, D. Esteve, and C. Urbina, Phys. Rev. Lett. **86**, 4104 (2001).
[39] F. Pauly, M. Dreher, J. K. Viljas, M. Häfner, J. C. Cuevas, and P. Nielaba, Phys. Rev. B **74**, 235106 (2006).
[40] We obtain the LDOS of atom i as $\mathrm{LDOS}_i(E) = -(1/\pi)\Sigma_\alpha \mathrm{Im}[\boldsymbol{S}_{CC}^{1/2}\boldsymbol{G}_{CC}^r(E)\boldsymbol{S}_{CC}^{1/2}]_{i\alpha,i\alpha}$, where α runs over all basis functions of that atom (Ref. 39). The LDOS of a region Ω containing several atoms is the sum over all atoms in this region, $\mathrm{LDOS}_\Omega(E) = \Sigma_{i\in\Omega}\mathrm{LDOS}_i(E)$.
[41] J. M. Krans, C. J. Muller, I. K. Yanson, Th. C. M. Govaert, R. Hesper, and J. M. van Ruitenbeek, Phys. Rev. B **48**, 14721 (1993).
[42] P. Jelínek, R. Pérez, J. Ortega, and F. Flores, Nanotechnology **16**, 1023 (2005).
[43] N. D. Lang, Phys. Rev. B **37**, 10395 (1988).
[44] A. Isambert and M. F. Goffman (private communication).
[45] A. R. Williams, P. J. Feibelman, and N. D. Lang, Phys. Rev. B **26**, 5433 (1982).
[46] M. Galperin, D. Segal, and A. Nitzan, J. Chem. Phys. **111**, 1569 (1999).
[47] For a different derivation, see, for example, T. N. Todorov, G. A. D. Briggs, and A. P. Sutton, J. Phys.: Condens. Matter **5**, 2389 (1993); and J. Ferrer, A. Martín-Rodero, and F. Flores, Phys. Rev. B **38**, 10113 (1988).
[48] M. Wolfsberg and L. Helmholz, J. Chem. Phys. **20**, 837 (1952).